Channel-specific aerosol rejections in IFS

Reima Eresmaa and Julie Letertre-Danczak
E-mail: r.eresmaa@ecmwf.int

January 29, 2019

1 Introduction

The operational NWP system of ECMWF is currently rejecting infrared (IR) radiances that are affected by either desert dust or volcanic ash aerosol (Letertre-Danczak, 2016). Aiming at accurately detecting contamination from desert dust, the applied method relies on observed brightness temperature (T_B) differences across the long-wave (LW) window region on both sides of the 9.6μm O_3 absorption band. The aerosol rejections were first implemented for the Infrared Atmospheric Sounding Interferometer (IASI) in the IFS cycle Cy41r2, that became operational in March 2016. The method was extended to Atmospheric Infrared Sounder (AIRS) and Cross-track Infrared Sounder (CrIS) in Cy43r1, becoming operational in November 2016. As no reliable method has been implemented to distinguish between affected and unaffected channels, the current practice is to reject all channels in the presence of aerosol in the sounder field-of-view (FOV). Because desert dust aerosol is often confined to lower troposphere, the chosen approach means under-exploitation of stratospheric- and upper-tropospheric-sensitive channels in those regions where dust outbreaks occur.

In addition to identifying the FOVs where aerosol is present, the observed T_B information is used to provide estimates of the aerosol optical depth (AOD). Currently these estimates are not routinely exploited, although they are of potential use in calculation of aerosol radiative forcing during the numerical forecast.

There has been recent work towards restricting the aerosol rejections to affected channels only. This work extends from the ECMWF cloud detection scheme (McNally and Watts, 2003), which assigns each channel with characteristic height indicative of the lower tail of the channel's weighting function. Applying statistical methods to first guess (FG) departure data, dynamical AOD-dependent rejection threshold is produced such that affected and unaffected channels can be separated from each other on the basis of their height assignments. This method basically makes the assumption that the top of

the aerosol layer increases monotonically with increasing AOD. The method is considered sufficiently mature for implementation in a future IFS version such as Cy47r1.

We provide a detailed description of the chosen method, including the calculation of AOD and conversion from AOD to rejection threshold, in Section 2. Subsequent sections focus on evaluating the method. The performance is evaluated in NWP context in Section 3 and against external aerosol retrievals in Section 4. We conclude the report with a summary in Section 5.

2 Method

2.1 Aerosol Optical Depth

The method applied for the aerosol detection in the IFS is based on the pioneering work of Peyridieu (2010) and Peyridieu et al. (2010), although exact details of the implementation are optimized for the use in the global NWP system of ECMWF. For each sounder, four channels are identified, using the V-shape of the infrared absorption spectrum for desert dust aerosol (Clarisse et al., 2013); wavenumbers of these are listed in Table 1. With CrIS and IASI, the effect of instrument noise is mitigated by averaging over several neighbouring channels around each wavenumber. Using the T_B observations at the four wavenumbers, differences Δ_{1-2} and Δ_{3-4} are formed and compared against fixed thresholds, as listed in Table 2. Presence of aerosol in the FOV is diagnosed if both of the two T_B differences are below the threshold values.

In the case of positive detection, AOD is estimated from the T_B difference Δ_{3-4} using the regression

$$AOD = \sum_{i=1}^{3} a_i \Delta_{3-4}^{i-1}, \quad (1)$$

where a_i are empirically-set coefficients, again set specifically for each sounder. The values used in the IFS are shown in Table 2. This empirical estimation of the AOD is again using the V-shape: the more aerosol in the FOV, the larger is the impact on the infrared spectrum. If presence of aerosol is not diagnosed, AOD is set to zero.

2.2 Determination of rejection threshold

Separating aerosol-affected channels from those not affected requires information, or making some reasonable assumptions, on each channel's height dependence and the vertical extent of the aerosol. For the height dependence, information is readily available in the form of height assignments, that are produced in preparation for the cloud detection. These depend on the model background and they indicate the altitude of a theoretical opaque cloud top that would alter the forward-modelled radiance by 1% of the clear-sky value. Using the height assignments, it becomes crucial to determine a threshold height, above which aerosol has a negligible impact on radiance observation.

In this work, an assumption is made that the top altitude of the aerosol layer increases with increasing AOD. Although likely to fail in some circumstances, the assumption

seems reasonable to start with, given that the origin of desert dust is at surface. With the goal being at deriving a useful definition for rejection threshold, it is helpful to study the behaviour of FG departure as a function of AOD on a handful of channels. Figure 1 exemplifies this approach for three IASI channels, that are sensitive to temperature at different altitudes. The scatterplots represent a known episode of Saharan dust off the west coast of North Africa in May 2017. Cloud-affected data is omitted from the sample.

At first glance, FG departure shows little dependence on AOD. We would expect increasing AOD to make departures increasingly negative, but such relationship is weak and it is found only in the case of the mid-tropospheric sounding channel (panel (b)). In panel (a), the slope of the linear least-square fit is practically zero, suggesting no measurable radiative effect from aerosol on the upper-tropospheric channel. In panel (c), the slope is positive and thus opposite to the expectation. The lack of expected behaviour here is possibly due to most of the aerosol-affected data being rejected during the cloud detection.

To get a clearer view to the effect AOD has on FG departure, Fig. 2 shows the slope of the linear least-square fit for all actively-used channels in LW CO_2 band of IASI. The x-axis is mean channel height assignment, normalized such that the highest- and lowest-ranked channels are at 0 and 1, respectively. Stratospheric and upper-tropospheric sounding channels cover approximately the range $0 \ldots 0.7$ along the x-axis. These channels show no clear sign of AOD dependence, as the slope is consistently either near zero or slightly positive (rather than negative). Range $0.7 \ldots 0.75$ potentially shows a feature of interest. Here, the slope of the least-square fit is negative and it increases in magnitude when channel sensitivity gets closer to surface. These channels have their primary sensitivities in mid-troposphere with weighting function peaks around 400–700 hPa. Further down, in the range $0.75 \ldots 1.0$, the slope appears more random, probably because of reduced samples of cloud-free data and also rejections of strongly affected data during the cloud detection.

Only considering the x-axis range $0.67 \ldots 0.75$, our next step is to least-squares fit a straight line through the data plotted in Fig. 2. This way we can super-parameterize the slope α as

$$\alpha \;=\; \beta + \gamma H, \tag{2}$$

where H is the normalized mean channel height assignment and fitted parameters are β=3.4311 and γ=-4.8548. Equation (2) can be employed as a predictor for the aerosol radiative effect δ such that

$$\delta \;=\; (\beta + \gamma H)\, AOD. \tag{3}$$

Assuming a value for δ, i.e. the maximum allowed aerosol radiative effect, we can solve the rejection threshold H_r from (3) as

$$H_r \;=\; \frac{1}{\gamma}\left(\frac{\delta}{AOD} - \beta\right). \tag{4}$$

For instance, setting δ=-0.01 K would yield the rejection threshold as indicated by the red line in Fig. 3. This specification would mean that the aerosol detection would

	T_1^B	T_2^B	T_3^B	T_4^B
AIRS	979.128	1228.23	1106.83	1230.81
CrIS	980.000±0.625	1232.50±1.25	1090.625±0.625	1233.75±1.25
IASI	979.75±1.25	1231.75±1.25	1090.25±1.25	1233.75±1.25

Table 1: Aerosol detection channel wavenumbers (in cm^{-1}). For CrIS, these correspond to the Nominal Spectral Resolution (NSR).

	t_{1-2}	t_{3-4}	a_1	a_2	a_3
AIRS	1.2	-5.0	-0.06	-0.001	0.002
CrIS	0.6	-1.2	-0.09	-0.06	0.01
IASI	0.2	-1.55	-0.18	-0.1	0.01

Table 2: Aerosol detection thresholds and AOD coefficients.

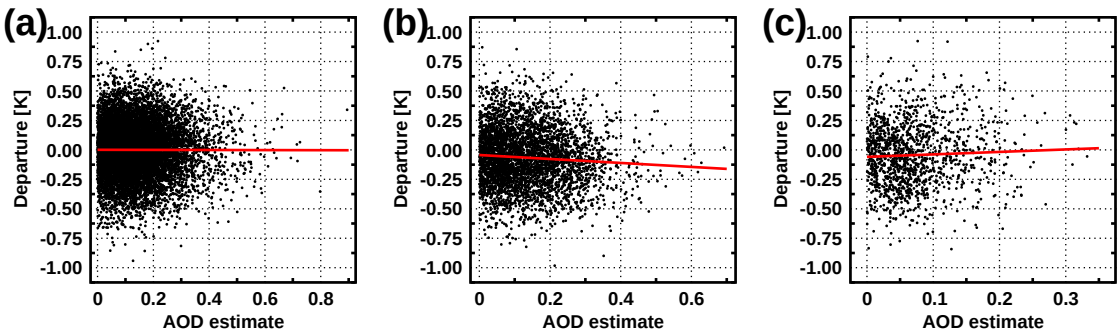

Figure 1: FG departure as a function of AOD on (a) an upper-tropospheric, (b) a mid-tropospheric, and (c) a lower-tropospheric sounding channel of IASI. Red lines indicate least-square-fitted linear regression.

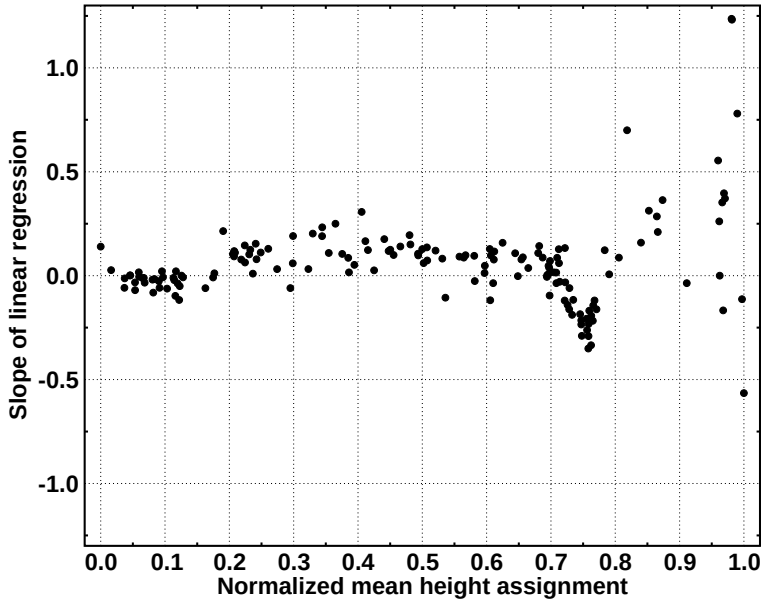

Figure 2: Slope of linear regression as a function of mean channel height assignment for long-wave CO_2 sounding and window channels of IASI. Higher (lower) ranked channels are to the left (right) along the x-axis.

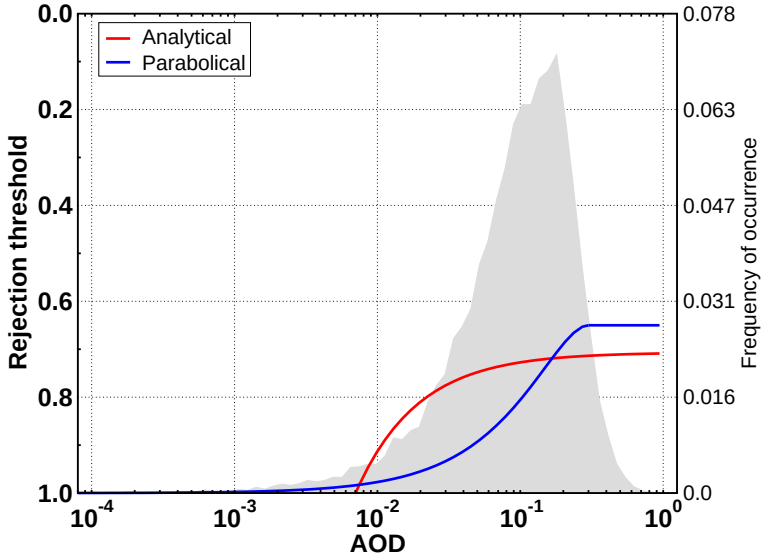

Figure 3: The two AOD-dependent rejection thresholds, expressed as normalized channel height assignment. Red and blue lines are for the analytical and parabolic thresholds, respectively. The shading shows the probability density function of AOD.

never reject any channel that is assigned normalized height less than 0.7. Furthermore, rejections become active only when AOD is greater than 0.007. There is little variation in the rejection threshold when AOD exceeds 0.05. Judging against the probability density function of AOD (gray shading), this would imply that the rejected subset of channels is nearly identical in most situations. In the remainder of this work, the definition (4), with parameter values set to δ=-0.01 K, β=3.4311, and γ=-4.8548, is referred to as the *analytical* threshold.

It should be emphasized that the analytical threshold results from applying statistical analysis on a spatially and temporally limited sample of FG departures. Practical constraints (such as limiting the analysis to cloud-free data only) in the derivation process make the robustness of the method somewhat questionable. For the sake of practical use in an operational data assimilation system, we have designed an alternative specification for testing in parallel with the analytical threshold. The alternative setup, hereafter *parabolic* threshold, is indicated by the blue line in Fig. 3 and it is formally defined as

$$H_r = \begin{cases} 1 & \text{when AOD} \leq 0 \\ a + bAOD + cAOD^2 & \text{when } 0 < \text{AOD} \leq 0.3 \\ 0.65 & \text{when AOD} > 0.3 \end{cases}$$

where coefficients are a=1.0, b=-2.333, and c=3.888. Admittedly, the parabolic threshold is very subjective, but it has certain convenient characteristics, such as providing substantial variation in the most populated range of AOD (i.e., between 0.1 ... 0.3) and rejecting some channels even when AOD is very low. The parabolic threshold is less cautious of the two for moderate values of AOD, but more cautious when AOD exceeds 0.1. This is hoped to improve the scheme's robustness for occurrence of AOD in excess of what is represented in the training dataset. In the next section, the two competing definitions are evaluated in terms of their performance in experimental NWP.

3 Evaluation in NWP framework

We have implemented the two rejection thresholds for testing in the IFS framework and evaluate their performance by applying standard verification tools on short- and medium-range forecasts. The following experiment runs are produced:

1. Control: As 45r1 e-suite (as of 14 March 2018), except with horizontal resolution reduced to TCo399 and with aerosol detection of AIRS and CrIS made approximately consistent with IASI. Positive detection of aerosol in IR FOV results in rejecting all channels.

2. No aerosol detection: As Control, except that the aerosol detection is switched off for all IR sounders.

3. Analytical threshold: As Control, except that positive detection of aerosol in IR FOV results in rejecting only channels ranked lower than the analytical threshold (i.e., red line in Fig. 3).

4. Parabolic threshold: As Control, except that positive detection of aerosol in IR FOV results in rejecting only channels ranked lower than the parabolic threshold (i.e., blue line in Fig. 3).

All of these runs are initialized at 00Z, 1 May 2017, and they initially cover the time period 1–31 May 2017. The control, analytical threshold, and parabolic threshold runs are extended further to additionally cover 1 June – 31 August 2017.

Figure 4 illustrates the effect of different rejection threshold specifications on count of active data. Data count is shown as a function of peak pressure of channel weighting function and it is normalized using the Control. Switching the aerosol detection off (black line) increases the data use by 4% in the stratosphere, by 7% in mid-troposphere, and by 3% on window channels. The increase in count of stratospheric channels is practically identical in the two runs with AOD-dependent rejection thresholds; it is less on tropospheric-peaking channels. With the analytical threshold (red line), the data count increase from the Control is nearly linear with height in troposphere, such that 4.5% more data are used on channels peaking around 400 hPa, while on window channels the increase is just 0.5%. With the the parabolic threshold (blue line), the excess data accounts for more than 4% throughout the upper- and mid-troposphere and goes down to around 1% on window channels.

Geographical distribution of added radiance data in the first month of the experiment is shown in left-hand-side panels of Fig. 5. The shading shows the increase in count of active data, relative to the Control, when considering all actively-used tropospheric-

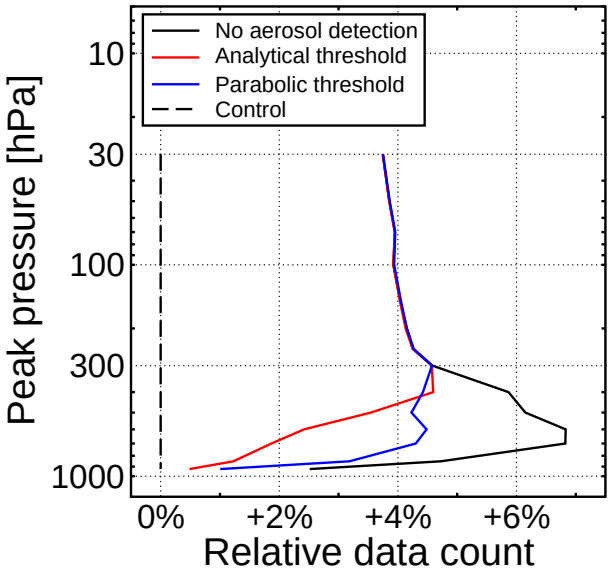

Figure 4: Count of active IASI data in May 2017 in the "No aerosol detection" (black), "Analytical threshold" (red), and "Parabolic threshold" runs, relative to the Control (black dashed).

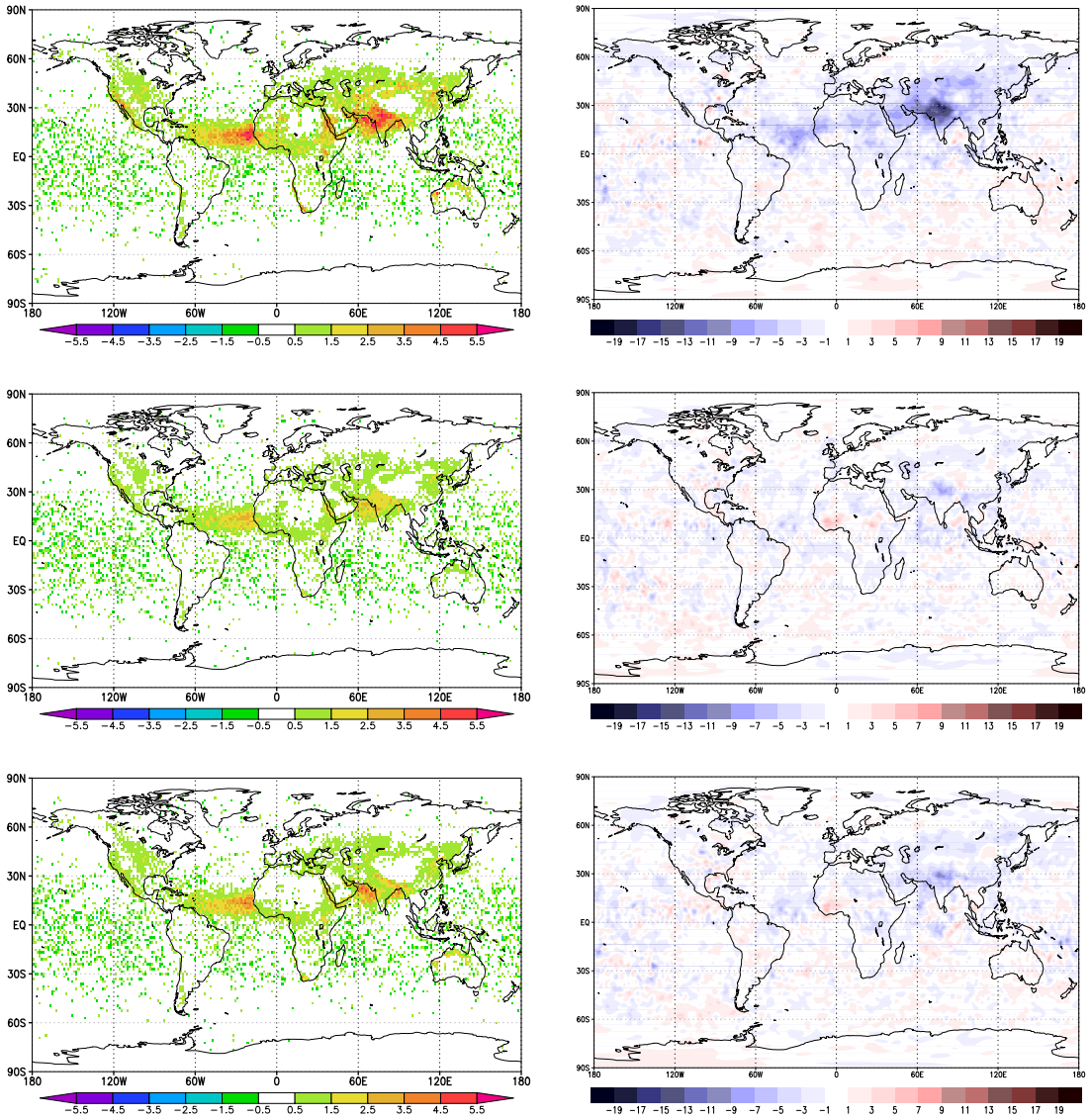

Figure 5: Count of active tropospheric-sensitive IASI data relative to Control (left; unit 1,000 observations) and mean 500 hPa geopotential height difference from Control (right; unit m^2s^{-2}) in May 2017. (top) No aerosol detection, (middle) Analytical threshold, and (bottom) Parabolic threshold.

peaking IASI channels in the LW band. Simply switching the aerosol detection off (top panel) produces the largest increase, that is most notable over sea near west coasts of North Africa and India and over Red Sea, but also over land areas at North American and Asian mid-latitudes. These are the regions where aerosol contamination occurs most frequently. Increases in the analytical and parabolic threshold runs are less prominent and concentrate more over sea, while data use changes over land are usually small. The right-hand-side panels of Fig. 5 show the impact the added data has on mean 500 hPa geopotential analysis. Completely ignoring the aerosol contamination cools the model atmosphere especially over Atlantic Ocean, Arabian Peninsula, and Middle East including Himalayas. The cooling is an indication of improper use of aerosol-contaminated radiances, and it is reassuring to find little such effect in the two runs where AOD-dependent rejections are made. The parabolic rejection run shows slightly more cooling than the analytical threshold run. This is to be expected as the use of data is more aggressive in the former.

Short-range forecast impact is evaluated using FG fit statistics on various independent observation types. Averaging over the whole globe and four Northern summer months (May–August), Fig. 6 shows control-normalized FG departure standard deviation for radiosonde observations of wind, temperature and specific humidity, as well as for geostationary IR radiances and microwave radiances of AMSU-A and MHS. While no convincing impact is found on wind- or temperature-sensitive data, there are indications of improved fit to humidity-sensitive observations. This is clearest with MHS in the Parabolic threshold run (blue line). The geostationary radiances, also primarily sensitive to upper-tropospheric humidity, provide further support on the idea of improvements in short-range humidity forecast. It is encouraging to find the positive FG fit impact to match the positions of the Meteosat (at 0^o and 42^oE) and GOES-13 (at 75^oW) satellites. Regions observed by these satellites are frequently affected by Saharan dust aerosol.

To summarize, of the two parallel implementations for the AOD-dependent rejection threshold, the parabolic threshold lets more tropospheric-sensitive IR data through, produces slightly more undesirable cooling to the mean analysis, and performs slightly better in terms of improving FG fit to independent humidity-sensitive data. Forecast impact from either one is neutral in this four-month experiment (not shown). On the basis of these results, we have chosen to propose the parabolic threshold for further experimentation, ultimately targeting operational implementation in a future IFS cycle.

4 Comparison with external aerosol products

In order to carry out an independent validation of the AOD and rejection threshold determination process outlined in Section 2, we have downloaded aerosol retrievals of the Atmospheric Radiation Analysis (ARA) team at Laboratoire de Meteorologie Dynamique (LMD; Capelle et al., 2018) for June 2017. The retrievals are provided separately for the two IASI's on Metop-A and Metop-B satellites and they are given as monthly means of AOD and aerosol layer altitude in a 0.5° latitude-longitude grid. Gridded retrievals are also available as daily maps, separated between day- and night-time overpasses.

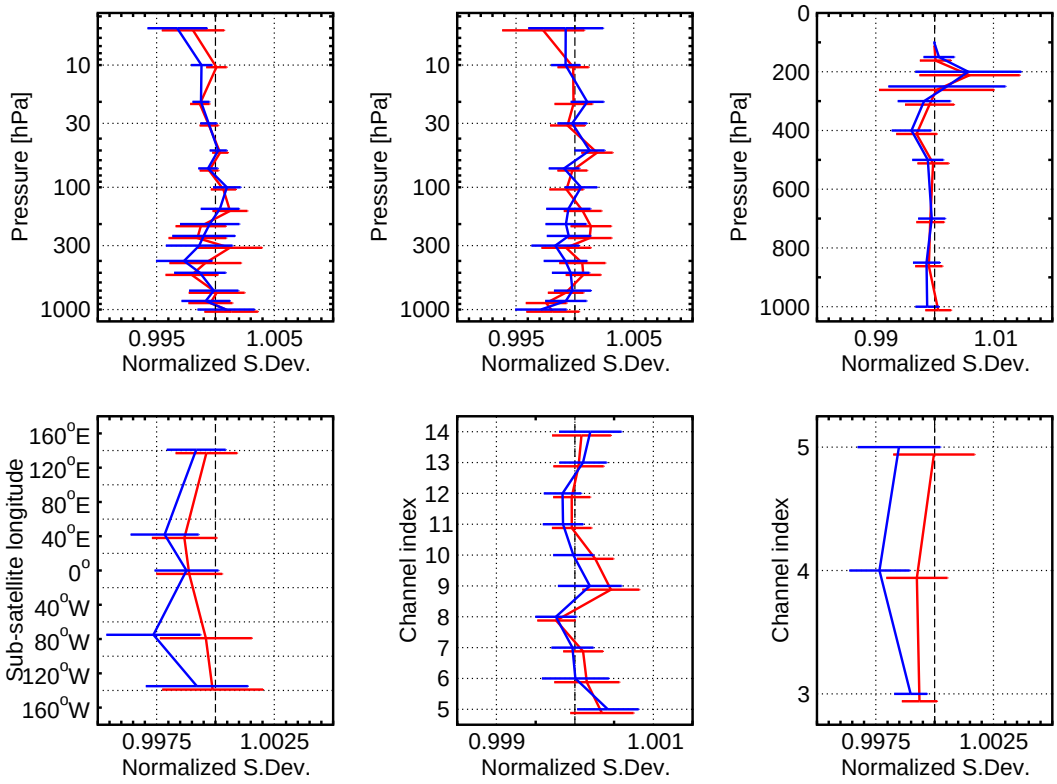

Figure 6: Impact of (partial) use of aerosol-affected FOVs on global observation to FG fit. Red (blue) shows the control-normalized standard deviation of FG departure for the analytical (parabolic) threshold run. The observation types included are (top left) radiosonde wind, (top middle) radiosonde temperature, (top right) radiosonde specific humidity, (bottom left) geostationary radiance, (bottom middle) AMSU-A radiance, and (bottom right) MHS radiance. Bars indicate 95% confidence intervals.

To ease the comparison, we have produced an experimental run that covers June 2017 and processes all IASI FOVs (rather than choosing just one out of each set of four, as would be the default). AOD is determined from all observations, although it is not necessarily meaningful in cases where aerosol is masked by cloud. We use the cloud flag on channel 269 (central wavenumber at 712 cm^{-1}; peak pressure at 440 hPa) as a proxy and produce a map of mean AOD from those FOVs, where this channel is clear of cloud. Qualifying estimates of AOD are accumulated over the month and mean AOD is calculated in the same horizontal grid that the LMD retrievals are given in.

Figure 7 shows the calculated mean AOD, plotted next to that retrieved from the database of LMD, for Metop-A and Metop-B IASI's in June 2017. In either dataset, differences between the two satellites are small. There is much more difference between the two datasets. As compared with the external product, the method of Section 2

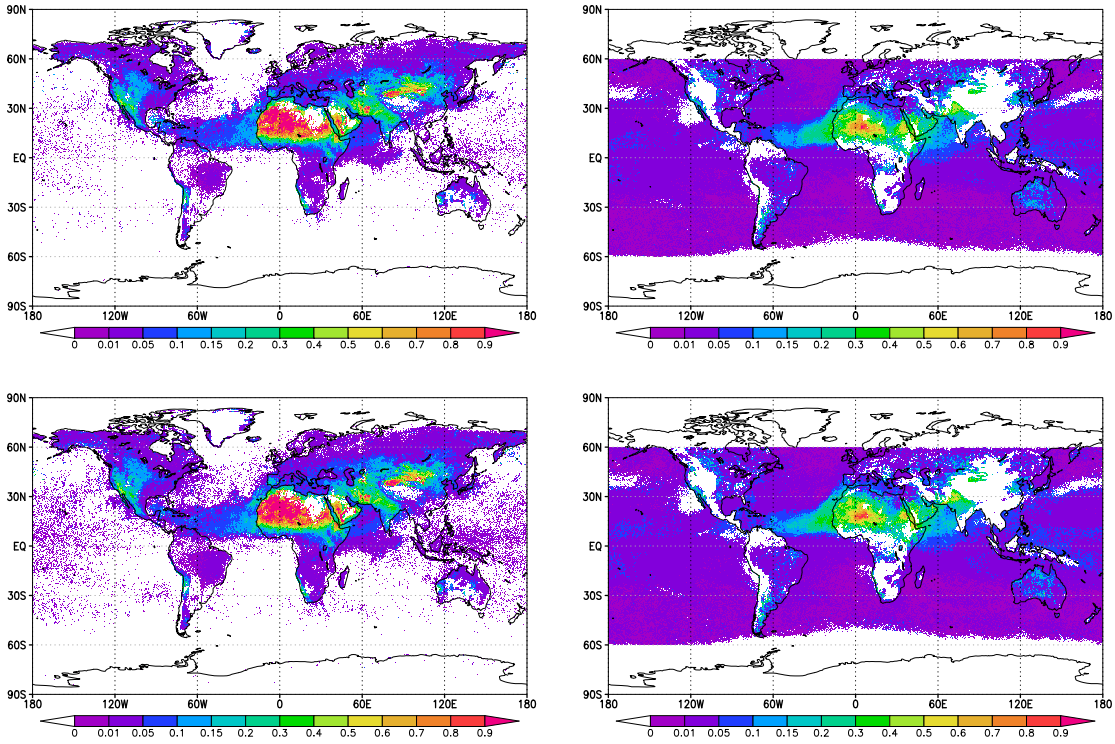

Figure 7: Gridded mean AOD as either calculated using the methods outlined in Section 2 (left) or retrieved from the database of ARA team at LMD (right). Metop-A (Metop-B) IASI is shown on the top (bottom) and the data is from 1–30 June 2017.

generally over-estimates AOD over land and under-estimates it over sea. The over-estimation is most obvious over Saharan desert and Arabian Peninsula. There are also areas of relatively large AOD above high ground around Rocky Mountains, Andes and Tibetian Plateau, where LMD retrievals are not available. The under-estimation is the worst at western parts of Atlantic Ocean and over Arabian sea.

In addition to the AOD, the LMD database includes gridded mean aerosol layer altitude that we use as a baseline for validating the parabolic rejection thresholds. Such validation is, however, not straightforward. On the one hand, the rejection threshold is designed to be sensitive to the top of the aerosol layer, rather than to the mean altitude archived in the LMD database. On the other hand, calculation of geometric height from the rejection threshold is complicated, as channel height assignments are expressed in the model vertical grid. In principle, the height assignments could be converted to geometric heights if temperature and humidity profiles (together with surface pressure) were known. In practice, model profiles are not saved at observation locations. Given these limitations, we take the following steps to estimate the top altitude of aerosol from the parabolic rejection threshold:

1. Convert the threshold H_r to model grid coordinates by inverting the normalization with maximum and minimum channel height assignments.

2. Interpolate from model vertical grid to geometric height using a look-up table that contains mean geometric height for each model level.

The look-up table is derived by integrating the hydrostatic equation for 3,486 sea-based profiles of the cloud-condensate-sampled subset in the 137-level IFS profile database (Eresmaa and McNally, 2014).

The gridded aerosol layer altitude derived this way for June 2017 is shown in Fig. 8 next to the mean aerosol layer altitude in the LMD database. As the parabolic threshold method assumes the layer altitude to increase monotonically with increasing AOD, mismatches between the two datasets are similar to those in the comparison of AOD. These are modulated by the fact that one of the two datasets indicates the top of the aerosol layer, while the other shows the mean altitude. As a result, the layer altitude as derived from the parabolic threshold appears grossly over-estimated over Saharan and Arabian land areas and under-estimated over sea in the western Atlantic and Indian Ocean. The best match is found over Atlantic Ocean immediately to the west off the coast of Africa.

According to the comparison with external products, there is some room for improving the estimates of AOD particularly over land surfaces. This alone would improve the consistency between IR channel rejections and independent aerosol products. Regardless of the quality of AOD estimates, though, potential will remain for further optimization in the area of identifying affected channels at each observation location. Ideally, this would mean relaxing the assumption of monotonically increasing dust layer altitude with increasing AOD. It needs to be emphasized at this point, however, that the main goal of future work should be kept in improved performance in the context of NWP.

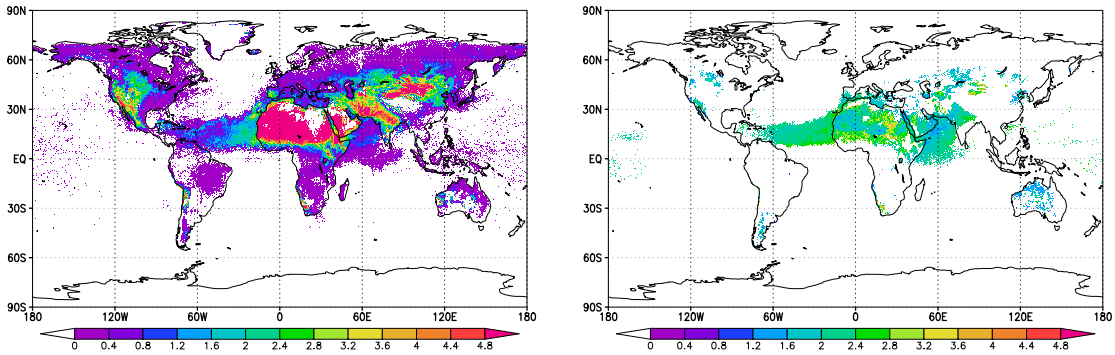

Figure 8: Gridded mean aerosol altitude as either calculated using the methods explained in Section 2 (left) or retrieved from the database of Laboratoire de Meteorologie Dynamique (right). Data is averaged over the two Metop satellites and it covers the time period of 1–30 June 2017.

5 Summary

We have designed a method for restricting aerosol-related IR data rejections to affected channels only. The method is intended to replace the current practice of rejecting all channels when aerosol is present in the FOV. The method relies on AOD as estimated from observed inter-channel T_B differences and it additionally takes advantage of channel height assignments, that are initially produced for use during the cloud detection.

The method makes a fundamental assumption that increasing aerosol layer altitude means increasing AOD. Working on a sample of FG departures, collected during a known episode of Saharan dust, we have used statistical tools to derive an analytical AOD-dependent threshold, against which individual channel height assignments are compared when making the aerosol-related data rejections. The used sample of FG departures consists of cloud-free data only. Consequently, there is an unfortunate complication that strongly aerosol-affected channels are left out of the process, as they tend to get rejected during the cloud detection. For convenience, and to respond to practical requirements of intended operational implementation, performance of the analytical threshold is compared not just against rejecting full spectra, but also against an alternative setup, called parabolic threshold. Although the parabolic threshold is more subjective than the analytical one, it produces a better impact on short-range forecasts, and is therefore proposed for operational implementation. Neither specification is found to produce a measurable impact on medium-range forecasts.

In comparison with external retrievals by the ARA team at LMD, the AOD estimates of this work are too high over land and too low over sea. This has an effect on the channel rejections such that the use of IR data is likely to be overly cautious (aggressive) over land (sea) surfaces. Further benefits could be achieved by making the AOD estimates more consistent between land and sea, as well as by increasing the level of sophistication in the way the affected channels are separated from unaffected ones.

References

Capelle V, A Chédin, M Pondrom, C Crevoisier, R Armante, L Crepeau, and N A Scott, 2018: Infrared dust aerosol optical depth retrieved daily from IASI and comparison with AERONET over the period 2007–2016. *Remote Sens. Environ.*, **206**, 15–32.

Clarisse L, P-F Coheur, F Prata, J Hadji-Lazaro, D Hurtmans, and C Clerbaux, 2013: A unified approach to infrared aerosol remote sensing and type specification. *Atmos. Chem. Phys.*, **13**, 2195–2221.

Eresmaa, R, and A McNally, 2014: Diverse profile datasets from the ECMWF 137-level short-range forecasts. *NWP SAF Report No. NWPSAF-EC-TR-017, 12 p.*

Letertre-Danczak J, 2016: The use of geostationary radiance observations at ECMWF and aerosol detection for hyper-spectral infrared sounders: 1st and 2nd years report. *EUMETSAT/ECMWF Fellowship Programme Research Report No. 40, 18 p.*.

McNally A and P Watts, 2003: A cloud detection algorithm for high-spectral-resolution infrared sounders. *Q. J. R. Meteorol. Soc.*, **129**, 3411–3423.

Peyridieu S, 2010: Etablissement d'une climatologie des propriétés des aérosols de poussières à partir d'observations hyperspectrales dans l'infrarouge. Application aux instruments AIRS et IASI. *Thèse de Doctorat, Université Pierre et Marie Curie, Paris, 240 p.*

Peyridieu S, A Chédin, D Tanré, V Capelle, C Pierangelo, N Lamquin, and R Armante, 2010: Saharan dust infrared optical depth and altitude retrieved from AIRS: A focus over North Atlantic - comparison to MODIS and CALIPSO. *Atmos. Chem. Phys.*, **10**, 1953–1967.